

Photoproduction of heavy quarks in ultraperipheral pp, pA, and AA collisions at the CERN Large Hadron Collider

Adeola Adelyi

Department of Physics & Astronomy, Texas A&M University-Commerce, Commerce, TX 75428, USA

Trang Nguyen

*Center for Nuclear Research, Department of Physics
Kent State University, Kent, OH 44242, USA*

(Dated: November 21, 2018)

Photoproduction of heavy quarks in ultraperipheral collisions can help elucidate important features of the physics of heavy quarks in Quantum Chromodynamics (QCD). Due to the dependence on parton distributions it can also potentially offer some constraining ability in the determination of nuclear parton distributions. In the present study we consider next-to-leading order (NLO) photoproduction of heavy quarks in ultraperipheral proton-proton (pp), proton-nucleus (pA), and nucleus-nucleus (AA) collisions at the CERN Large Hadron Collider (LHC). Total cross sections and rapidity distributions are considered and the influence of nuclear modifications of parton distributions on these quantities are explored for pA and AA collisions. We find that photoproduction of heavy quarks in PbPb collisions exhibit significant sensitivity to nuclear effects, and in conjunction with photoproduction in pPb collisions, affords good constraining potential for gluon shadowing determination.

PACS numbers: 24.85.+p, 25.30.Dh, 25.75.-q

I. INTRODUCTION

The study of ultraperipheral relativistic heavy ion collisions is useful in exploring several aspects of particle and nuclear physics and is an important part of current experimental efforts at the LHC. Consequently ultraperipheral collisions have been extensively discussed in the literature (for a small sample of references, see e.g. [1–13]) for different collision systems and various photon-nucleus and photon-photon processes.

In [14–16] we have considered photoproduction of $c\bar{c}$ and $b\bar{b}$ in ultraperipheral pPb ($\sqrt{s_{NN}} = 5$ TeV and $\sqrt{s_{NN}} = 8.8$ TeV) and PbPb ($\sqrt{s_{NN}} = 2.76$ TeV and $\sqrt{s_{NN}} = 5.5$ TeV) collisions at the LHC. A major shortcoming was that the results were calculated to leading order (LO) in perturbative QCD. In this article we remedy this shortcoming and present results at next-to-leading order (NLO) accuracy. We also consider, as an addition to the previous treatments, photoproduction of heavy quarks in ultraperipheral pp collisions at $\sqrt{s_{NN}} = 7$ TeV and $\sqrt{s_{NN}} = 14$ TeV. As in the earlier studies an important goal is to investigate quantitatively the influence of nuclear modifications of parton distributions on observables such as cross sections and rapidity distributions and also the extent of applicability of these observables in helping to constrain components of nuclear parton distributions.

The paper is organized as follows: in Sec. II we discuss photoproduction of heavy quarks and the basic ingredients required in our calculations, namely photon flux, photohadron cross sections, and input nuclear and photon parton distributions. In Sec. III we present the results of our calculations. Our conclusion is contained in Sec. IV.

II. PHOTON-HADRON INTERACTIONS IN ULTRAPERIPHERAL COLLISIONS

In general the total cross section for the photoproduction of a pair of heavy quarks ($c\bar{c}$ or $b\bar{b}$) in ultraperipheral collisions can be expressed as a convolution of the incident photon flux, dN_γ/dk , with the energy-dependent photo-cross section $\sigma^{\gamma H \rightarrow Q\bar{Q}}(k)$, with k denoting the photon energy and H a proton or nucleus. Thus for pp collisions we can write

$$\sigma_{pp}^{Q\bar{Q}} = 2 \int dk \frac{dN_\gamma^p(k)}{dk} \sigma^{\gamma p \rightarrow Q\bar{Q}}(k), \quad (1)$$

with dN_γ^p/dk the photon flux from a proton in the pp collision system and $\sigma^{\gamma p \rightarrow Q\bar{Q}}(k)$ the energy-dependent cross section for the photoproduction of a $Q\bar{Q}$ pair off a proton. The factor of 2 accounts for the source/target symmetry present in symmetric collisions, since each proton can act simultaneously as a source and target of photons. A similar expression holds for AA collisions with dN_γ^p/dk replaced with dN_γ^Z/dk , the flux from one of the participating nuclei and $\sigma^{\gamma p \rightarrow Q\bar{Q}}(k)$ replaced with $\sigma^{\gamma A \rightarrow Q\bar{Q}}(k)$, the cross section for photoproduction of a $Q\bar{Q}$ pair off a nucleus. In the case of pA collisions the nucleus acts preferentially as the source and the proton as the target, leading predominantly to γp processes. But there is still a non-negligible contribution from γA processes in which the proton acts as the source of photons and the nucleus as the target. Thus expressions for both types of fluxes are required for pA collisions. We can thus write

$$\sigma_{pA}^{Q\bar{Q}} = \int dk \left[\frac{dN_\gamma^Z}{dk} \sigma^{\gamma p \rightarrow Q\bar{Q}}(k) + \frac{dN_\gamma^p}{dk} \sigma^{\gamma A \rightarrow Q\bar{Q}}(k) \right], \quad (2)$$

with dN_γ^Z/dk and dN_γ^p/dk the fluxes from the nucleus and proton in the pA collision system and $\sigma^{\gamma p \rightarrow Q\bar{Q}}(k)$ and $\sigma^{\gamma A \rightarrow Q\bar{Q}}(k)$ the photonucleon and photonuclear cross sections respectively.

Manifestations of nuclear effects can be more transparently observed when rapidity distributions are considered. Using the relation $d\sigma/dy = kd\sigma/dk$ the pair rapidity distribution can be expressed as

$$\frac{d\sigma^{\gamma H \rightarrow Q\bar{Q}}}{dy} = k \frac{dN_\gamma(k)}{dk} \sigma^{\gamma H \rightarrow Q\bar{Q}}(k) \quad (3)$$

and scales directly with the photon flux dN_γ/dk . Thus for pA collisions, with the convention that the proton is incident from the right and the nucleus from the left, the total rapidity distribution is

$$\begin{aligned} \frac{d\sigma^{pA \rightarrow Q\bar{Q}}}{dy} &= \left[k \frac{dN_\gamma^Z(k)}{dk} \sigma^{\gamma p \rightarrow Q\bar{Q}}(k) \right]_{k=k_l} \\ &+ \left[k \frac{dN_\gamma^p(k)}{dk} \sigma^{\gamma A \rightarrow Q\bar{Q}}(k) \right]_{k=k_r} \end{aligned} \quad (4)$$

where k_l ($k_l \propto e^{-y}$) and k_r ($k_r \propto e^y$) simply denote photons from the nucleus and proton respectively. The first term on the right-hand side (γp distribution) peaks at positive rapidities while the second term (γA distribution) peaks at negative rapidities. Since both the fluxes and cross sections are different, the total distribution is manifestly asymmetric, and the γp term dominates due to the much larger nuclear flux dN_γ^Z/dk .

The total rapidity distribution for AA collisions can likewise be written as

$$\begin{aligned} \frac{d\sigma^{AA \rightarrow Q\bar{Q}}}{dy} &= \left[k \frac{dN_\gamma^Z(k)}{dk} \sigma^{\gamma A \rightarrow Q\bar{Q}}(k) \right]_{k=k_l} \\ &+ \left[k \frac{dN_\gamma^Z(k)}{dk} \sigma^{\gamma A \rightarrow Q\bar{Q}}(k) \right]_{k=k_r} \end{aligned} \quad (5)$$

with k_l and k_r simply denoting photons from the nucleus incident from the left and right respectively. Here the cross sections and the left/right fluxes are identical; thus the first term on the right-hand side of Eq. (5) yields a distribution which is the mirror image of the second term. Consequently the total distribution is symmetric about midrapidity ($y = 0$). Similar expression and symmetry attribute hold true for pp collisions.

A. Photon flux

Let us now consider the various photon fluxes occurring in the expressions for total cross sections and rapidity distributions. For a given impact parameter \mathbf{b} , the flux of virtual photons with photon energy k , $d^3N_\gamma(k, \mathbf{b})/dkd^2b$, is strongly dependent on the Lorentz factor γ . The photon flux also depends strongly on the

adiabaticity parameter $\zeta = kb/\gamma$ [2–4]:

$$\frac{d^3N_\gamma(k, \mathbf{b})}{dkd^2b} = \frac{Z^2\alpha\zeta^2}{\pi^2kb^2} \left[K_1^2(\zeta) + \frac{1}{\gamma^2} K_0^2(\zeta) \right], \quad (6)$$

which drops off exponentially for $\zeta > 1$, above a cutoff energy determined essentially by the size of the nucleus, $E_{cutoff} \sim \gamma \text{MeV}/b$ (fm).

The photon flux from a proton is usually estimated using the dipole formula for the electric form factor [17]:

$$\begin{aligned} \frac{dN_\gamma^p(k)}{dk} &= \frac{\alpha}{2\pi k} \left[1 + \left(1 - \frac{2k}{\sqrt{s_{NN}}} \right)^2 \right] \\ &\left(\ln D - \frac{11}{6} + \frac{3}{D} - \frac{3}{2D^2} + \frac{1}{3D^3} \right), \end{aligned} \quad (7)$$

where $D = 1 + [0.71 \text{ GeV}^2/Q_{\min}^2]$ and the minimum momentum transferred $Q_{\min}^2 = k^2/[\gamma^2(1 - 2k/\sqrt{s_{NN}})]$.

In the case of proton-nucleus (pA) collisions, the flux from the proton is given by Eq. (7) while the flux due to the nucleus (of charge Z) can be evaluated analytically and is given by [2],

$$\begin{aligned} \frac{dN_\gamma^Z(k)}{dk} &= \frac{2Z^2\alpha}{\pi k} \left[\zeta_R^{pA} K_0(\zeta_R^{pA}) K_1(\zeta_R^{pA}) \right. \\ &\left. - \frac{(\zeta_R^{pA})^2}{2} (K_1^2(\zeta_R^{pA}) - K_0^2(\zeta_R^{pA})) \right], \end{aligned} \quad (8)$$

with reduced adiabaticity parameter, ζ_R^{pA} , given by $\zeta_R^{pA} = k(R_p + R_A)/\gamma$ and R_p the effective radius of the proton.

For nucleus-nucleus (AA) collisions an analytic approximation similar to Eq. (8) can be derived. A more accurate expression for the flux can be obtained by integrating $d^3N_\gamma(k, \mathbf{b})/dkd^2b$ over impact parameters with the constraint of no hadronic interactions and accounting for the photon polarization. This yields the total photon flux $dN_\gamma^Z(k)/dk$ given by [5, 11],

$$\begin{aligned} \frac{dN_\gamma^Z(k)}{dk} &= 2\pi \int_{2R_A}^\infty db b \int_0^R \frac{dr r}{\pi R_A^2} \int_0^{2\pi} d\phi \\ &\times \frac{d^3N_\gamma(k, b + r \cos \phi)}{dkd^2b}, \end{aligned} \quad (9)$$

with R_A the radius of the nucleus.

B. Photoproduction cross sections

In general photon interactions with hadrons and nuclei can be classified as direct or resolved. In direct interactions the photon behave as a point-like particle while in resolved interactions the incident photon first fluctuates into a quark-antiquark state (or an even more complex partonic configuration consisting of quarks and gluons) which then subsequently interacts hadronically with the hadron or nuclear target. The cross section for the photoproduction of a pair of heavy quarks, $\sigma^{\gamma H \rightarrow Q\bar{Q}}(k)$, is

therefore a sum of both the direct and resolved contributions:

$$\sigma^{\gamma H \rightarrow Q\bar{Q}}(k) = \sigma_{direct}^{\gamma H \rightarrow Q\bar{Q}}(k) + \sigma_{resolved}^{\gamma H \rightarrow Q\bar{Q}}(k). \quad (10)$$

Here H stands for a proton or a nucleus ($H \equiv p, A$) and the total photoproduction cross section is obtained by convolution of the energy-dependent cross section $\sigma^{\gamma H \rightarrow Q\bar{Q}}(k)$ and the equivalent photon flux, $dN_\gamma(k)/dk$, as given in Eq. (1) for symmetric pp (AA) collisions and Eq. (2) for asymmetric pA collisions.

Let us consider both contributions in some detail. In view of the high energies involved perturbative QCD is applicable, and both the direct and resolved contributions are expressible as convolution of the cross sections for the relevant partonic subprocesses and the corresponding nucleon/nuclear parton distributions. Thus the direct contribution can be written as

$$\sigma_{direct}^{\gamma H \rightarrow Q\bar{Q}}(s) = \sum_{a=q,\bar{q},g} \int dx_a \sigma^{\gamma a \rightarrow Q\bar{Q}}(x_a s, Q^2) \times f_a^H(x_a, Q^2) \Theta(\zeta_a). \quad (11)$$

Here $\sigma^{\gamma a \rightarrow Q\bar{Q}}(x_a s, Q^2)$ is the parton-level cross section for the photoproduction of a heavy quark pair from the interaction of a photon γ and a parton a with momentum fraction x_a . The renormalization scale, μ_r , has been set equal to the factorization scale, μ_f i.e. $\mu_r = \mu_f = Q$ and $f_a^H(x_a, Q^2)$ is the parton distribution of a in H evaluated at x_a and Q^2 . In addition $s = W_{\gamma H}^2$ denotes the square of the center-of-mass energy of the photon-nucleus (or photon-nucleon) system, $\hat{s} = W_{\gamma a}^2 = x_a s$ that of the photon-parton system, and $\zeta_a = \hat{s} - 4m_Q^2$ with m_Q the mass of the heavy quark (charm or bottom). The function $\Theta(\zeta_a)$ enforces a minimum (“threshold”) value of x_a , x_a^{min} , on the integral given by $x_a^{min} = 4m_Q^2/s$. Note that the summation over q involves only the light flavors, i.e. $q = u, d, s$.

The resolved contribution is similar in structure to hadroproduction of heavy quarks and can be written as

$$\sigma_{resolved}^{\gamma H \rightarrow Q\bar{Q}}(s) = \sum_{a,b=q,\bar{q},g} \int dx_a dx_b \sigma^{ab \rightarrow Q\bar{Q}}(x_a x_b s, Q^2) \times f_a^\gamma(x_a, Q^2) f_b^H(x_b, Q^2) \Theta(\zeta_{ab}), \quad (12)$$

where $\sigma^{ab \rightarrow Q\bar{Q}}(x_a x_b s, Q^2)$ is the partonic $ab \rightarrow Q\bar{Q}$ cross section, $f_a^\gamma(x_a, Q^2)$ ($f_b^H(x_b, Q^2)$) is the distribution of parton a (b) with momentum fraction x_a (x_b) in a photon (H) respectively, $\hat{s} = x_a x_b s$ and $\zeta_{ab} = \hat{s} - 4m_Q^2$. Similar to the direct contribution, the summation over q involves only light quark flavors, i.e. $q = u, d, s$.

It is thus clear that the two major ingredients needed for the determination of the hadronic photoproduction cross sections are the partonic (parton-level) cross sections and parton distributions in nucleon/nuclei and photons. Below we briefly discuss them.

1. Partonic cross sections

Photon-gluon fusion is the only relevant subprocess for the direct contribution at leading order (LO), and the expression for the cross section can be found in [18–20]. In the case of LO resolved contribution, only the gg and $q\bar{q}$ channels are relevant, and the corresponding cross sections can be found in [21–23]. We have used the next-to-leading order (NLO) results presented in [24, 25] for both direct and resolved contributions. Small- x effects (see [26]) which could potentially be important for charm photoproduction are not addressed in the present study. These effects should be somewhat lessened in the case of the resolved contribution due to the inherent small- x cut-off ($x > 0.001$) present in the photon parton distributions used in this work.

2. Parton distributions in nuclei and photons

We now turn to the consideration of the parton distributions (PDs) relevant to the processes considered in the present study. While the direct contribution to the photoproduction of heavy quarks requires the distributions of light quarks/antiquarks and gluons in protons and nuclei, the resolved contribution, in addition, requires these distributions in photons also. Thus in addition to the usual requirement of nucleon and nuclear parton distributions (nPDs), there is also the need for the relatively poorly known parton distributions in photons (γ PDs), thereby increasing the level of the theoretical uncertainties in the calculation of photoproduction of heavy quarks.

Let us first discuss nuclear parton distributions. It is rather well-known that the distributions of partons (i.e. quarks and gluons) in nuclei are quite different from the distributions in free nucleons, that is, they are “modified” by the complex, many-body effects in the nucleus. These nuclear effects are usually parametrized in terms of “nuclear modifications” $R_a^A(x, Q^2)$ which in general depend on the parton specie (a), the nucleus (A), momentum fraction x and scale Q^2 . The nuclear effects can be categorized based on different intervals in x . At small values of x ($x \lesssim 0.04$), we have the phenomenon generally referred to as shadowing. This is a depletion, in the sense that in this interval, the distribution of a parton a in the nucleus is smaller compared to the corresponding distribution in a free proton, i.e. $R_a^A < 1$. Antishadowing, which is an enhancement ($R_a^A > 1$), occurs in the range $0.04 \lesssim x \lesssim 0.3$. Another depletion, the classic EMC effect [27], is present in the interval $0.3 \lesssim x \lesssim 0.8$, while for $x > 0.8$, the Fermi motion region, we have another enhancement. It is important to note that although both shadowing and the EMC effect (antishadowing and Fermi motion) correspond to depletion (enhancement), the physical principles and mechanisms governing these phenomena are quite different. Further details can be found in [28–31] With the knowledge of $R_a^A(x, Q^2)$, nuclear parton distributions can be expressed as a convo-

lution of free nucleon parton distributions and nuclear modifications, i.e. $f_a^A(x, Q^2) = f_a(x, Q^2) \otimes R_a^A(x, Q^2)$.

While the determination of quark and antiquark distributions in nucleons and nuclei is in general a nontrivial task, that of gluons is even more problematic. Gluons are electrically neutral, and thus their distributions cannot be extracted directly from Deeply Inelastic Scattering (DIS) and Drell-Yan (DY) processes which account for the major part of the data used in global fits. Their distributions are in general inferred from sum rules and the Q^2 evolution of sea quarks distributions. The situation is even worse in the nuclear case: the available data is much less than for nucleons, and there is the added complication of a mass dependence. It is therefore not unusual for nuclear gluon distributions from different global fits to differ significantly, especially in the magnitude of the various nuclear effects (shadowing, antishadowing, etc). This is especially obvious at low Q^2 (i.e. around their initial starting scales) since evolution to high Q^2 tends to lessen the differences. Earlier global analyses [32–35] relied heavily on fixed-target nuclear deep-inelastic scattering (DIS) and Drell-Yan (DY) lepton-pair production data. Incorporation of additional data from inclusive hadron production in deuteron-gold collisions and neutrino-iron processes has been implemented in [36–41]. The approach in [42, 43] utilizes the Gribov picture of shadowing and data from diffractive processes to generate nuclear modifications. Despite all these advances the nuclear gluon distribution is still currently the least constrained aspect of nuclear parton distributions, as significant uncertainties still persist at both small and large x .

Three recent nucleon/nuclear parton distributions are utilized in the present study. For the proton we use the Martin-Stirling-Thorne-Watts (MSTW08) parton distributions [44] which are available up to next-to-next-to-leading order (NNLO). In the nuclear case we use two nuclear modification sets: the NLO set by Eskola, Paukunen, and Salgado (EPS09) [37] and the NLO set by Frankfurt, Guzey, and Strikman (FGS10) [43]. For EPS09 we use the central fit while for FGS10 we use the strong gluon shadowing model (FGS10_H). The distributions from MSTW08 serve two purposes: as the free nucleon distributions used in conjunction with nuclear modifications, and also as a “special” nuclear distribution in the absence of nuclear effects. The latter case is particularly useful for highlighting the influence of the various nuclear effects on observables.

It is instructive to compare the characteristics of the light partons and gluon distributions from both EPS09 and FGS10 sets based on the strength of their nuclear modifications. In Fig. 1 we show the nuclear modifications for light quarks and gluons in Pb, $R_f^{Pb}(x, Q^2)$ from EPS09 and FGS10 at the factorization scale $Q^2 = 4m_c^2$. For valence up (u_v) and down (d_v) quarks, both distributions exhibit identical antishadowing, EMC, and Fermi motion characteristics. Both u_v and d_v are less shadowed in FGS10 than in EPS09 for the entire shadowing interval

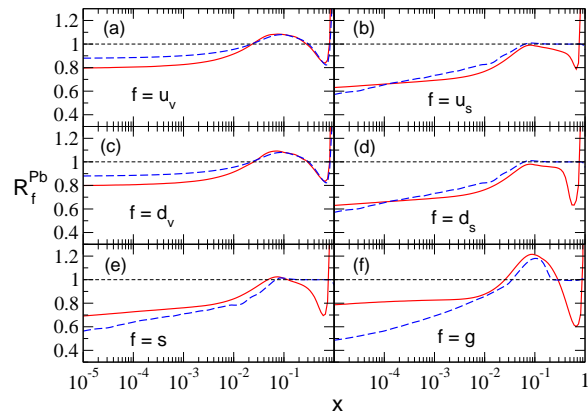


FIG. 1. (Color online) Nuclear modifications of light quarks and gluons in Pb, $R_f^{Pb}(x, Q^2 = 4m_c^2 \text{ GeV}^2)$, from EPS09 (solid line) and FGS10H (dashed line): (a) valence up quark u_v , (b) up sea quark u_s ($\equiv \bar{u}$), (c) valence down quark d_v , (d) down sea quark d_s ($\equiv \bar{d}$), (e) strange quark s ($\equiv \bar{s}$), and (f) gluon g .

(≈ 0.9 versus 0.8 at very small x). In the case of \bar{u} and \bar{d} , the EMC and Fermi motion effects which are present in EPS09 are virtually absent in FGS10. The shadowing components are not very different, with FGS10 being slightly more shadowed at very small x , and EPS09 more shadowed for $x > 10^{-4}$. In FGS10 strange quarks (antiquarks) are more shadowed but there is an absence of EMC and Fermi motion characteristics which are present in EPS09. By far the most impressive difference occurs in the shadowing of the gluon sector: the gluon shadowing in EPS09 is almost constant at small x at ≈ 0.8 while in FGS10 the shadowing increases with decreasing x , reaching a value of about 0.49 at $x \approx 10^{-5}$. While EPS09 exhibits both EMC and Fermi motion effects these are absent in FGS10. Also the antishadowing component is smaller in FGS10 than in EPS09. Thus in the shadowing regime it is reasonable to expect that much of the differences in the predictions from EPS09 and FGS10 stem from their radically different gluon characteristics.

Parton distributions in photons (γ PDs) are derived from experimentally determined photon structure function $F_2^\gamma(x, Q^2)$, in conjunction with appreciable theoretical inputs. These inputs, which are necessary in implementing the parametrization of photon parton distributions from the structure function, account in part for some of the observable differences in the available photon parton distribution sets. Another source of differences is in the choice and scope of experimental data from which F_2^γ is extracted. At present there is an appreciable number of photon parton distribution sets available, both at leading and next-to-leading orders [45–61]. It should be noted that unlike in the case of a nucleon, there are no valence quarks present in the photon; therefore

antiquark distributions are the same as quark distributions. Furthermore, there are no sum rules governing the gluon content; thus the gluon distribution is almost totally unconstrained. The gluon distribution contributes to $F_2^\gamma(x, Q^2)$ majorly through the $\gamma^*g \rightarrow q\bar{q}$ channel, which has significant numerical support only at small x .

Two recent NLO photon parton distributions are the set by Cornet, Jankowski, and Krawczyk (CJK04) [60] and that by Aurenche, Fontannaz, and Guillet (AFG04) [61]. The CJK04 set uses the DIS renormalization scheme while the MSbar scheme is employed in AFG04. We have used the AFG04 set (AFG04_BF) in the present study for consistency with the renormalization scheme used in [24, 25] for the NLO cross sections used in this work. In Fig. 2 we show the parton distributions from the AFG04 NLO set for the light (u,d,s) quarks and gluon. The most

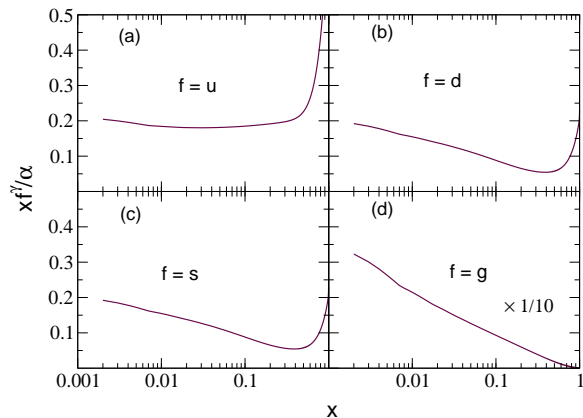


FIG. 2. (Color online) Parton distributions in the photon for (a) up, (b) down, (c) strange quarks, and (d) gluons at $Q^2 = 4m_c^2$ GeV² from the AFG04 distribution set. For better visuality the gluon distribution (d) has been scaled down by a factor of 10.

remarkable characteristic is the dramatic rise of g^γ with decreasing x .

III. RESULTS

We now discuss the results of our calculations for the inclusive photoproduction of heavy quarks ($c\bar{c}$ and $b\bar{b}$) in ultraperipheral proton-proton (pp), proton-lead (pPb), and lead-lead (PbPb) collisions at the LHC. The calculations are carried out at two center-of-mass (cms) energies for each collision system: E_1^{pp} ($\sqrt{s_{NN}} = 7$ TeV) and E_2^{pp} ($\sqrt{s_{NN}} = 14$ TeV) for pp, E_1^{pPb} ($\sqrt{s_{NN}} = 5$ TeV) and E_2^{pPb} ($\sqrt{s_{NN}} = 8.8$ TeV) for pPb, and E_1^{PbPb} ($\sqrt{s_{NN}} = 2.76$ TeV) and E_2^{PbPb} ($\sqrt{s_{NN}} = 5.5$ TeV) for PbPb collisions respectively. We take $m_c = 1.4$ GeV and $m_b = 4.75$ GeV for consistency with the MSTW08 parton distributions. The strong coupling constant at scale

Q^2 , $\alpha_s(Q^2)$, is evaluated to two loops using the evolution code contained in the MSTW08 package. For $c\bar{c}$ we set $Q^2 = 4m_c^2$ while for $b\bar{b}$ we take $Q^2 = m_b^2$.

A. Heavy quarks in pp collisions

In Table I we show the cross sections for the direct and resolved components, as well as their sum, for the photoproduction of $c\bar{c}$ and $b\bar{b}$ in ultraperipheral pp collisions at the two specified cms energies.

TABLE I. Direct, resolved, and total cross sections for photoproduction of $c\bar{c}$ and $b\bar{b}$ in ultraperipheral pp collisions at the LHC. All cross sections are in nanobarns (nb).

	$\sqrt{s_{NN}}$ (TeV)	Direct	Resolved	Total
$c\bar{c}$	7	2050.9	677.1	2728.0
	14	2837.6	1124.7	3962.3
$b\bar{b}$	7	31.2	20.1	51.3
	14	52.8	44.0	96.8

Some interesting features can be deduced from Table I. Thus at $\sqrt{s_{NN}} = 7$ TeV the resolved contribution is about 24.8% of the total cross section for $c\bar{c}$ and 39.1% for $b\bar{b}$, while at $\sqrt{s_{NN}} = 14$ TeV the resolved component accounts for 28.4% and 45.5% respectively for $c\bar{c}$ and $b\bar{b}$ production. It is thus evident that the resolved contribution, being a significant fraction of the total cross section, is important for $c\bar{c}$, and more especially so for $b\bar{b}$ production, with this importance increasing with increasing energy.

These features are apparent in the rapidity distributions for $c\bar{c}$ as shown in Fig. 3, and for $b\bar{b}$ as displayed in Fig. 4. These distributions are manifestly symmetric about midrapidity ($y = 0$) due to the source/target symmetry present in pp collisions.

It is instructive to explore how the cross sections scale with energy. To this end we consider the ratio of the total cross section at $\sqrt{s_{NN}} = 14$ TeV to that at $\sqrt{s_{NN}} = 7$ TeV for both $c\bar{c}$ (denoted by $R_{c\bar{c}}$) and $b\bar{b}$ (denoted by $R_{b\bar{b}}$) production. From Table I we can see that $R_{c\bar{c}} = 1.452$ and $R_{b\bar{b}} = 1.887$ respectively. Thus for $c\bar{c}$ the total cross section at $\sqrt{s_{NN}} = 14$ TeV is approximately 1.5 times larger than at $\sqrt{s_{NN}} = 7$ TeV, and approximately 1.9 times larger in the case of $b\bar{b}$ production. This implies that the cross section for $b\bar{b}$ production grows more rapidly with increasing energy. Componentwise the ratio of direct cross sections is ≈ 1.4 for $c\bar{c}$ and ≈ 1.7 for $b\bar{b}$ while for resolved it is ≈ 1.7 and ≈ 2.2 respectively.

B. Heavy quarks in pPb collisions

Photoproduction in ultraperipheral pPb collisions arise from two distinct processes: γp interactions in which the Pb nucleus is the source of the photon and the proton acts as the target, and γPb interactions in which the

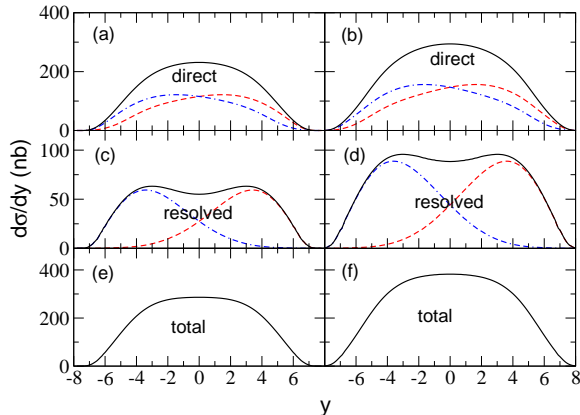


FIG. 3. (Color online) Rapidity distributions of $c\bar{c}$ photo-production in ultraperipheral pp collisions at the LHC. Solid lines in (a), (c), and (e) depict the direct, resolved, and total distributions at $\sqrt{s_{NN}} = 7$ TeV while solid lines in (b), (d), and (f) are the equivalent distributions at $\sqrt{s_{NN}} = 14$ TeV. In the two upper rows dashed and dash-dotted lines denote contributions from photons incident from the left and right respectively.

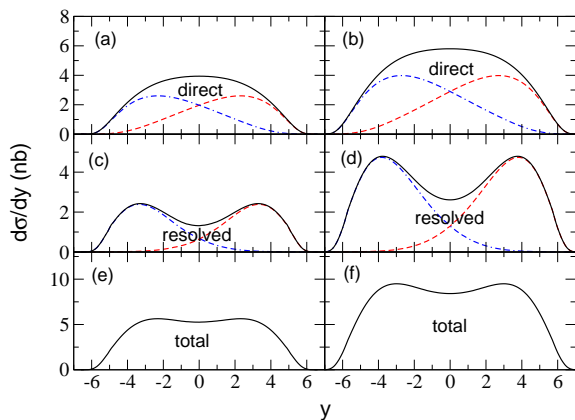


FIG. 4. (Color online) Rapidity distributions of $b\bar{b}$ photo-production in ultraperipheral pp collisions at the LHC. Solid lines in (a), (c), and (e) depict the direct, resolved, and total distributions at $\sqrt{s_{NN}} = 7$ TeV while solid lines in (b), (d), and (f) are the equivalent distributions at $\sqrt{s_{NN}} = 14$ TeV. In the two upper rows dashed and dash-dotted lines denote contributions from photons incident from the left and right respectively.

proton is the source of photons and the Pb nucleus is the target. Due to the large disparity in the magnitude of the photon fluxes from the proton and the nucleus (Pb) the γp contribution dominates, and a common practice is to neglect the photonuclear (γPb) contribution. We retain

the photonuclear contribution in this study and test the severity of the approximation made in neglecting it.

In Table II we present the cross sections for the direct and resolved components of both γp and γPb contributions for $c\bar{c}$ and $b\bar{b}$ production in ultraperipheral pPb collisions at the LHC. Total cross sections for both $c\bar{c}$ and $b\bar{b}$ are presented in Table III.

TABLE II. Direct and resolved cross sections for photoproduction of $c\bar{c}$ and $b\bar{b}$ in ultraperipheral pPb collisions at the LHC. All cross sections are in microbarns (μb).

		PDF	$\sqrt{s_{NN}} = 5$ TeV		$\sqrt{s_{NN}} = 8.8$ TeV	
			Direct	Resolved	Direct	Resolved
$c\bar{c}$	γp	MSTW08	2474.6	462.2	3563.5	823.8
	γPb	MSTW08	179.6	53.8	238.2	84.0
		EPS09	157.9	48.7	207.2	74.4
		FGS10	131.9	46.5	169.5	70.5
$b\bar{b}$	γp	MSTW08	21.4	6.4	38.0	15.1
	γPb	MSTW08	2.5	1.4	3.9	2.7
		EPS09	2.3	1.4	3.6	2.6
FGS10		2.1	1.3	3.2	2.6	

Let us first consider $c\bar{c}$ production. At $\sqrt{s_{NN}} = 5$ TeV the γPb contribution to the total cross section is approximately 7.4% for MSTW08 (no nuclear modifications), 6.6% for EPS09 (moderate gluon shadowing), and 5.7% for FGS10 (strong gluon shadowing) respectively. The resolved component accounts for 16.3% of total cross sections, and is independent of the choice of parton distribution set. Overall the sensitivity to nuclear modifications (dominantly shadowing) is very small: the no-modification (MSTW08) total cross section is reduced by approximately 0.9% and 1.7% by the modifications in EPS09 and FGS10 respectively.

The trend is similar at $\sqrt{s_{NN}} = 8.8$ TeV. Here the γPb contribution to the total cross section is approximately 6.8% for MSTW08, 6% for EPS09, and 5.2% for FGS10 respectively. The resolved component yields approximately 19.3% of total cross sections, and is also independent of the choice of parton distribution set. Identically the sensitivity to nuclear modifications remains the same as at $\sqrt{s_{NN}} = 5$ TeV.

These features are reflected in Fig. 5 where we show the component as well as total rapidity distributions at $\sqrt{s_{NN}} = 5$ TeV and $\sqrt{s_{NN}} = 8.8$ TeV respectively. In accordance with our convention the γp contribution peaks at positive rapidities while the γPb distributions peak at negative rapidities, and the asymmetric nature of the total distributions is clearly exhibited. Due to the smallness of the γPb contribution, the effects of nuclear modifications are totally negligible in the total rapidity distributions as the distributions from the three different parton distribution sets practically overlap.

We now discuss the case for $b\bar{b}$ production. In line with the treatment of $c\bar{c}$ production, we determine the relative importance of γPb and resolved contributions to the total $b\bar{b}$ production cross sections. At $\sqrt{s_{NN}} = 5$ TeV the γPb contribution to the total cross section is approx-

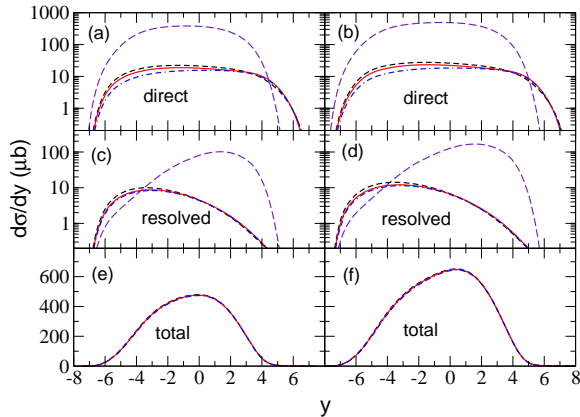


FIG. 5. (Color online) Rapidity distributions of $c\bar{c}$ photoproduction in ultraperipheral pPb collisions at the LHC. In (a), (c), and (e) we show the direct, resolved, and total distributions at $\sqrt{s_{NN}} = 5$ TeV while (b), (d), and (f) display the equivalent distributions at $\sqrt{s_{NN}} = 8.8$ TeV. In the first and second rows long-dashed line depicts the γp component while short-dashed (MSTW08), solid (EPS09), and dash-dotted (FGS10) lines correspond to γPb component with no shadowing, moderate shadowing, and strong shadowing respectively. In the third row short-dashed, solid, and dash-dotted lines depict total distributions using MSTW08, EPS09, and FGS10 parton distributions respectively.

imately 12.1% for MSTW08, 11.6% for EPS09, and 11% for FGS10 respectively. It is immediately apparent that at this energy the γPb contributions are more significant than their counterparts in $c\bar{c}$ production, and also less sensitive to nuclear effects. The resolved component is responsible for 24.6% of total cross sections and is independent of the choice of parton distribution set. The sensitivity to nuclear modifications is smaller than in $c\bar{c}$ production: the no-modification (MSTW08) total cross section is reduced by approximately 0.05% and 1.2% respectively by the modifications in EPS09 and FGS10 parton distribution sets.

TABLE III. Total cross sections for photoproduction of $c\bar{c}$ and $b\bar{b}$ in ultraperipheral pPb collisions at E_1^{pPb} ($\sqrt{s_{NN}} = 5$ TeV) and E_2^{pPb} ($\sqrt{s_{NN}} = 8.8$ TeV). All cross sections are in microbarns (μb).

PDF	$c\bar{c}$			$b\bar{b}$		
	E_1^{pPb}	E_2^{pPb}	$R_{c\bar{c}}$	E_1^{pPb}	E_2^{pPb}	$R_{b\bar{b}}$
MSTW08	3170.3	4709.5	1.486	31.6	59.8	1.894
EPS09	3143.4	4668.9	1.485	31.4	59.4	1.891
FGS10	3115.3	4627.3	1.485	31.2	59.0	1.892

Similar features are present at $\sqrt{s_{NN}} = 8.8$ TeV. The γPb contribution to the total cross section here is approximately 11.1% for MSTW08, 10.4% for EPS09, and 9.8% for FGS10 respectively. Again these values are rel-

atively more significant than those obtained in $c\bar{c}$ production. The resolved component accounts for approximately 30% of total cross sections, and is again independent of the choice of parton distribution set. The sensitivity to nuclear modifications are similar to those obtained at $\sqrt{s_{NN}} = 5$ TeV: 0.07% for EPS09 and 1.4% for FGS10 respectively.

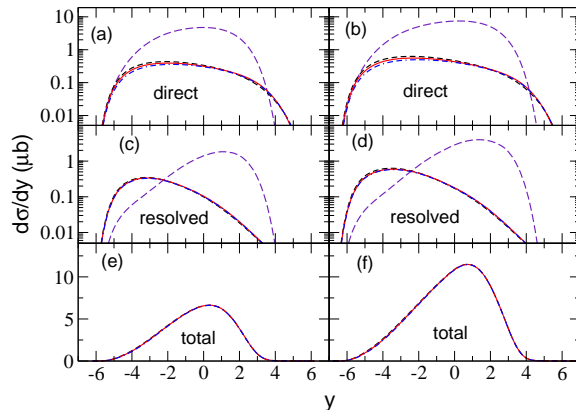


FIG. 6. (Color online) Rapidity distributions of $b\bar{b}$ photoproduction in ultraperipheral pPb collisions at the LHC. In (a), (c), and (e) we show the direct, resolved, and total distributions at $\sqrt{s_{NN}} = 5$ TeV while (b), (d), and (f) display the equivalent distributions at $\sqrt{s_{NN}} = 8.8$ TeV. In the first and second rows long-dashed line depicts the γp component while short-dashed (MSTW08), solid (EPS09), and dash-dotted (FGS10) lines correspond to γPb component with no shadowing, moderate shadowing, and strong shadowing respectively. In the third row short-dashed, solid, and dash-dotted lines depict total distributions using MSTW08, EPS09, and FGS10 parton distributions respectively.

In Fig. 6 we show the component as well as total rapidity distributions for $b\bar{b}$ production at $\sqrt{s_{NN}} = 5$ TeV and $\sqrt{s_{NN}} = 8.8$ TeV respectively. These distributions faithfully manifest the features described above. As in $c\bar{c}$ production the γp contribution peaks at positive rapidities while the γPb distributions peak at negative rapidities, the total distributions being thus asymmetric due to the dominance of the γp contribution. The effects of nuclear modifications on total rapidity distributions are totally negligible, as the distributions from the three different parton distribution sets practically overlap. This is due to the fact that even though the γPb contributions are relatively larger, they are also almost totally insensitive to nuclear effects.

Let us now discuss the magnitude of the change in cross section with energy. In Table III we present the ratio of the total cross section at $\sqrt{s_{NN}} = 8.8$ TeV to that at $\sqrt{s_{NN}} = 5$ TeV for $c\bar{c}$, $R_{c\bar{c}}$, and for $b\bar{b}$, $R_{b\bar{b}}$. As can be seen from Table III $R_{c\bar{c}} \approx 1.5$ and $R_{b\bar{b}} \approx 1.9$ for all three parton distribution sets. These values are practically the same as obtained for pp collisions.

C. Heavy quarks in PbPb collisions

We now discuss production of $c\bar{c}$ and $b\bar{b}$ in ultraperipheral PbPb collisions at energies $\sqrt{s_{NN}} = 2.76$ TeV and $\sqrt{s_{NN}} = 5.5$ TeV. In Table IV we show the cross sections for both direct and resolved components while total cross sections are presented in Table V

TABLE IV. Direct and resolved cross sections for photoproduction of $c\bar{c}$ and $b\bar{b}$ in ultraperipheral PbPb collisions at the LHC. All cross sections are in millibarns (mb).

	PDF	$\sqrt{s_{NN}} = 2.76$ TeV		$\sqrt{s_{NN}} = 5.5$ TeV	
		Direct	Resolved	Direct	Resolved
$c\bar{c}$	MSTW08	552.6	69.5	926.2	161.5
	EPS09	517.6	69.6	845.9	156.9
	FGS10	475.7	67.6	755.4	152.0
$b\bar{b}$	MSTW08	3.24	0.60	7.52	2.06
	EPS09	3.30	0.64	7.40	2.14
	FGS10	3.18	0.62	7.10	2.10

Due to both participants being nuclei, nuclear effects are more pronounced in PbPb collisions than in pPb collisions. Thus the resolved components, which in pPb collisions are quite independent of the choice of parton distribution set, and so by implication insensitive to nuclear effects, now acquire some sensitivity in PbPb collisions. Total cross sections and rapidity distributions also exhibit enhanced sensitivity.

As usual let us first consider $c\bar{c}$ production. At $\sqrt{s_{NN}} = 2.76$ TeV the resolved components are 11.2%, 11.9%, and 12.5% respectively for MSTW08, EPS09, and FGS10 distribution sets. In addition, the MSTW08 total cross section is reduced by 5.6% and 12.7% respectively by the nuclear modifications in EPS09 and FGS10 sets.

The same trend is observed at $\sqrt{s_{NN}} = 5.5$ TeV. Here the resolved components are 14.9% (MSTW08), 15.6% (EPS09), and 16.8% (FGS10) respectively. The influence of shadowing is more appreciable; the no-modification MSTW08 total cross section is reduced by 7.8% (EPS09) and 16.6% (FGS10) respectively.

These features are manifested in the rapidity distributions shown in Fig. 7. The distributions are symmetric about midrapidity ($y = 0$) as expected for symmetric collision systems. Also the sensitivity to nuclear modifications is more transparent here than in total cross sections.

Shadowing is the dominant nuclear effect for $-2.5 < y < 2.5$ at $\sqrt{s_{NN}} = 2.76$ TeV and for $-3 < y < 3$ at $\sqrt{s_{NN}} = 5.5$ TeV. The rapidity distributions in these intervals reproduce the observed trend of gluon shadowing strength exhibited in Fig. 1. MSTW08 with its zero gluon shadowing gives the largest rapidity distribution while FGS10H, with its strong gluon shadowing, gives the smallest. Due to strong flux suppression, shadowing is most markedly apparent for the rapidity range $-1.5 \lesssim y \lesssim 1.5$ for $\sqrt{s_{NN}} = 2.76$ TeV and $-2 \lesssim y \lesssim 2$ for $\sqrt{s_{NN}} = 5.5$ TeV. These intervals are therefore particularly suited for constraining purposes and also for dis-

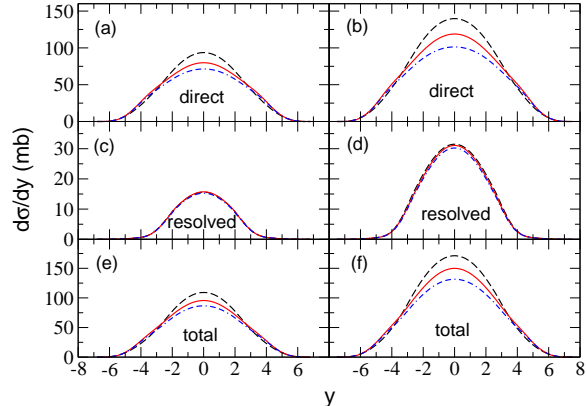


FIG. 7. (Color online) Rapidity distributions of $c\bar{c}$ photoproduction in ultraperipheral PbPb collisions at the LHC. In (a), (c), and (e) we show the direct, resolved, and total distributions respectively at $\sqrt{s_{NN}} = 2.76$ TeV while (b), (d), and (f) denote the equivalent distributions at $\sqrt{s_{NN}} = 5.5$ TeV. In all cases long-dashed (MSTW08), solid (EPS09), and dash-dotted (FGS10) lines correspond to no shadowing, moderate shadowing, and strong shadowing respectively.

criminating among different gluon shadowing scenarios.

At $\sqrt{s_{NN}} = 2.76$ TeV the rapidity intervals $2.5 < y < 5$ corresponds to x_{min} in the antishadowing region (deep shadowing) for right (left) incident photons and vice versa for $-5 < y < -2.5$. Due to the photon flux suppression in the deep shadowing region, the rapidity distributions are sensitive mainly to antishadowing in addition to both EMC effect and Fermi motion. Since both EPS09 and FGS10H have substantial antishadowing, their rapidity distributions reflect this, being slightly larger than those from MSTW08. The discriminatory power here is not as appreciable as in the shadowing case though, due largely to the smallness of the distributions. This is also the case for the rapidity intervals $3 < y < 6$ and $-6 < y < -3$ at $\sqrt{s_{NN}} = 2.76$ TeV.

TABLE V. Total cross sections for photoproduction of $c\bar{c}$ and $b\bar{b}$ in ultraperipheral PbPb collisions at E_1^{PbPb} ($\sqrt{s_{NN}} = 2.76$ TeV) and E_2^{PbPb} ($\sqrt{s_{NN}} = 5.5$ TeV). All cross sections are in millibarns (mb).

PDF	$c\bar{c}$			$b\bar{b}$		
	E_1^{PbPb}	E_2^{PbPb}	$R_{c\bar{c}}$	E_1^{PbPb}	E_2^{PbPb}	$R_{b\bar{b}}$
MSTW08	622.0	1087.7	1.75	3.9	9.6	2.49
EPS09	587.2	1002.8	1.71	3.9	9.5	2.42
FGS10	543.3	907.3	1.67	3.8	9.2	2.41

Let us now consider the corresponding case of $b\bar{b}$ production in ultraperipheral PbPb collisions. The sensitivity to nuclear modifications, while more appreciable here than in pPb collisions, is significantly less than for the equivalent $c\bar{c}$ production. At $\sqrt{s_{NN}} = 2.76$ TeV the

resolved components are 15.7%, 16.2%, and 16.3% respectively for MSTW08, EPS09, and FGS10 distribution sets. Thus to a good approximation the resolved component can be taken as 16% for all three parton distribution sets. It is noteworthy that unlike what obtains in $c\bar{c}$ production at this energy, both the direct and resolved components from EPS09 are the largest. In addition the resolved component from FGS10 is also larger than that of MSTW08. This is due to the increasingly important role of antishadowing at this energy. Thus the EPS09 total cross section is 2.2% larger than that of MSTW08. Due to the stronger shadowing and smaller antishadowing in FGS10, the total cross section is approximately 1.1% smaller.

At $\sqrt{s_{NN}} = 5.5$ TeV the resolved components are respectively 21.5% for MSTW08, 22.4% for EPS09, and 22.9% for FGS10. While the influence of shadowing can be seen in the direct components, both EPS09 and FGS10 yield larger resolved components, again due to antishadowing. Thus the MSTW08 total cross section is reduced by 0.6% and 4.4% by EPS09 and FGS10 respectively.

In Fig. 8 we show the corresponding rapidity distributions. Considering the left-hand panels ($\sqrt{s_{NN}} = 2.76$

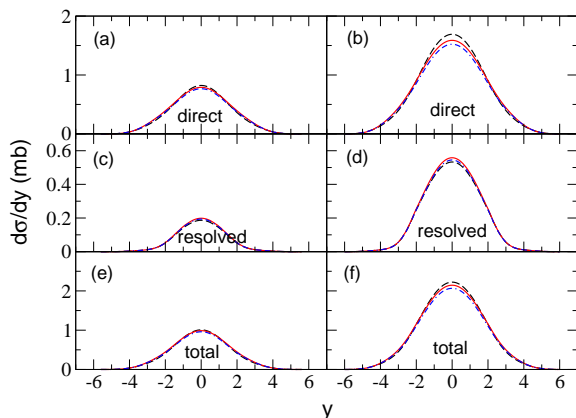


FIG. 8. (Color online) Rapidity distributions of $b\bar{b}$ photoproduction in ultraperipheral PbPb collisions at the LHC. In (a), (c), and (e) we show the direct, resolved, and total distributions respectively at $\sqrt{s_{NN}} = 2.76$ TeV while (b), (d), and (f) denote the equivalent distributions at $\sqrt{s_{NN}} = 5.5$ TeV. In all cases long-dashed (MSTW08), solid (EPS09), and dash-dotted (FGS10) lines correspond to no shadowing, moderate shadowing, and strong shadowing respectively.

TeV), it is apparent that the influence of shadowing present in the direct component in the rapidity interval $-1 < y < 1$ is almost totally negated by the antishadowing dominant in the same interval in the resolved component, with the result that in this interval total rapidity distributions have very little sensitivity to nuclear effects. For $-3 < y < -1$ and $1 < y < 3$ the slight manifestation of antishadowing seen in the direct component persists

in the total distributions.

These features are also present in the distributions at $\sqrt{s_{NN}} = 5.5$ TeV. Here also the clear influence of shadowing in the rapidity interval $-2 < y < 2$ in the direct component is reduced by the antishadowing present in the resolved component in the same interval. Thus the total rapidity distribution exhibit reduced sensitivity to nuclear shadowing in this interval due to this destructive interference. Nevertheless the influence of shadowing is still apparent especially in the rapidity window $-1 < y < 1$. Thus this interval presents the best sensitivity to shadowing effects in $b\bar{b}$ production. As at the lower energy, there is a slight manifestation of antishadowing in the intervals $-4 < y < -2$ and $2 < y < 4$.

Let us now consider the magnitude of the change in cross section with energy. In Table V we present the ratio of the total cross section at $\sqrt{s_{NN}} = 5.5$ TeV to that at $\sqrt{s_{NN}} = 2.76$ TeV for $c\bar{c}$, $R_{c\bar{c}}$, and for $b\bar{b}$, $R_{b\bar{b}}$. As is readily apparent from the Table, both $R_{c\bar{c}}$ and $R_{b\bar{b}}$ vary slightly with the choice of parton distribution set. Despite this variation, to a good approximation $R_{c\bar{c}} \approx 1.7$ and $R_{b\bar{b}} \approx 2.4$ for all three parton distribution sets. These values are larger, especially for $R_{b\bar{b}}$ than obtained for both pp and pPb collisions.

D. Theoretical errors and ratio of cross sections

From a consideration of the general structure of the quantities (cross sections and rapidity distributions) considered in this study, three major sources of theoretical errors can be readily identified:

- accuracy of the relevant expressions for photon flux,
- higher-order corrections,
- uncertainties in parton distributions.

Due to technical reasons we have not attempted to estimate quantitatively the uncertainties on calculated quantities in the present study. A pragmatic approach to facilitate shadowing determination is to compare photoproduction in proton-nucleus and nucleus-nucleus collisions, where many theoretical uncertainties and systematic errors cancel (see for instance [8, 13]). Here we explore in a rather simplistic and nonrigorous manner such an approach for shadowing effects in $c\bar{c}$ and $b\bar{b}$ photoproduction. We are primarily interested in relative effects, and as such issues like exact normalization and flux parallelism have been ignored.

In Fig. 9 we show the ratio $\sigma^{PbPb}/(208\sigma^{pPb})$ as a function of rapidity for both $c\bar{c}$ and $b\bar{b}$ in their respective shadowing regions. In order to have nearly identical Lorentz factor γ the PbPb cross sections, σ^{PbPb} , have been calculated at $\sqrt{s_{NN}} = 5.5$ TeV and the pPb cross sections, σ^{pPb} , at $\sqrt{s_{NN}} = 5$ TeV. It should be noted that in our calculations equal rapidity corresponds to equal photon energy.

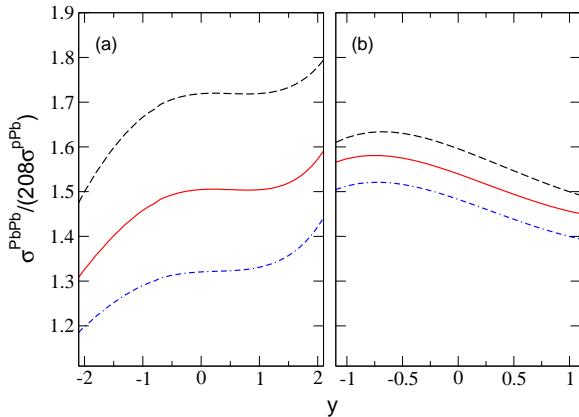


FIG. 9. (Color online) Ratio of photoproduction cross sections, $\sigma^{PbPb}/(208\sigma^{pPb})$, in the shadowing region for (a) $c\bar{c}$ and (b) $b\bar{b}$. The PbPb collisions are at $\sqrt{s_{NN}} = 5.5$ TeV while the pPb collisions are at $\sqrt{s_{NN}} = 5$ TeV. In both panels long-dashed (MSTW08), solid (EPS09), and dash-dotted (FGS10) lines correspond to no shadowing, moderate shadowing, and strong shadowing respectively.

Let us compare the shadowing effects from these ratios at a specific rapidity, say at $y = 0$. Thus for $c\bar{c}$ the MSTW08 value is reduced by approximately 12.5% and 23.2% respectively by the shadowing in EPS09 and FGS10. These reductions are precisely what one obtains from the rapidity distributions of $c\bar{c}$ in PbPb collisions at $\sqrt{s_{NN}} = 5.5$ TeV. This is also true for $b\bar{b}$ where the ratio reduction values 3.5% (EPS09) and 7.1% (FGS10) are the same as from the rapidity distributions. It thus seems feasible, at least in this simplistic case, that relative shadowing effects are transmitted without appreciable loss. Of course, in order to ascertain to what degree higher or-

der effects are cancelled in these ratios, one should carry out the analogous calculations at leading order. Further work along this line is in progress.

IV. CONCLUSIONS

In the present study we have considered next-to-leading order (NLO) photoproduction of $c\bar{c}$ and $b\bar{b}$ in ultraperipheral proton-proton (pp), proton-lead (pPb) and lead-lead (PbPb) collisions at LHC. In addition to its value in probing several aspects of QCD dynamics, photoproduction of heavy quarks can also aid in elucidating and constraining some components of nuclear parton distributions. Although the parton distribution dependence is linear and different modifications are superimposed due to the integration over parton momentum fraction x , both cross sections and rapidity distributions for $c\bar{c}$ in PbPb collisions manifest appreciable sensitivity to shadowing around midrapidity and a slight sensitivity to antishadowing at more forward and backward rapidities. Thus $c\bar{c}$ photoproduction offers good constraining potential for shadowing, and a somewhat less potential for antishadowing. Despite the fact that photoproduction of $b\bar{b}$ is less sensitive to nuclear modifications than $c\bar{c}$, the influence of shadowing is evident around midrapidity, and it thus offers some constraining ability for shadowing. Both $c\bar{c}$ and $b\bar{b}$ total photoproduction cross sections and rapidity distributions in pPb collisions show little sensitivity to nuclear modifications and are therefore useful in shadowing determination via cross section ratios. In addition their resolved components are appreciable, especially for $b\bar{b}$ and thus it seems feasible that they could be of some use in constraining photon parton distributions.

We thank C.A. Bertulani and M.J. Murray for helpful suggestions.

-
- [1] E. Fermi, Z. Physik **29**, 315 (1924); Nuovo Cimento **2**, 143 (1925).
[2] C. A. Bertulani and G. Baur, Phys. Rep. **163**, 299 (1988).
[3] R. N. Cahn and J. D. Jackson, Phys. Rev. D **42**, 3690 (1990).
[4] G. Baur and L. G. Ferreira Filho, Nucl. Phys. A **518**, 786 (1990).
[5] S. Klein and J. Nystrand, Phys. Rev. C **60**, 014903 (1999).
[6] C. A. Bertulani and D. S. Dolci, Nucl. Phys. A **674**, 527 (2000).
[7] V. P. Goncalves and C. A. Bertulani, Phys. Rev. C **65**, 054905 (2002).
[8] S. R. Klein, J. Nystrand and R. Vogt, Phys. Rev. C **66**, 044906 (2002).
[9] V. P. Goncalves and M. V. T. Machado, Eur. Phys. J. C **31**, 371 (2003).
[10] C. A. Bertulani, S. R. Klein and J. Nystrand, Ann. Rev. Nucl. Part. Sci. **55**, 271 (2005).
[11] A. J. Baltz *et al.*, Phys. Rept. **458**, 1 (2008).
[12] A. L. Ayala Filho, V. P. Goncalves and M. T. Griep, Phys. Rev. C **78**, 044904 (2008).
[13] C. A. Salgado, J. Alvarez-Muniz, F. Arleo, N. Armesto, M. Botje, M. Cacciari, J. Campbell and C. Carli *et al.*, J. Phys. G **39**, 015010 (2012).
[14] A. Adeluyi and C. Bertulani, Phys. Rev. C **84**, 024916 (2011).
[15] A. Adeluyi and C. A. Bertulani, Phys. Rev. C **85**, 044904 (2012).
[16] A. Adeluyi, C. A. Bertulani and M. J. Murray, arXiv:1208.6258 [nucl-th].
[17] M. Drees and D. Zeppenfeld, Phys. Rev. D **39**, 2536 (1989).
[18] M. Gluck and E. Reya, Phys. Lett. B **79**, 453 (1978).
[19] L. M. Jones and H. W. Wyld, Phys. Rev. D **17**, 759 (1978).

- [20] H. Fritzsche and K. H. Streng, Phys. Lett. B **72**, 385 (1978).
- [21] M. Gluck, J. F. Owens and E. Reya, Phys. Rev. D **17**, 2324 (1978).
- [22] B. L. Combridge, Nucl. Phys. B **151**, 429 (1979).
- [23] R. Brock *et al.* [CTEQ Collaboration], Rev. Mod. Phys. **67**, 157 (1995).
- [24] R. K. Ellis and P. Nason, Nucl. Phys. B **312**, 551 (1989).
- [25] P. Nason, S. Dawson and R. K. Ellis, Nucl. Phys. B **303**, 607 (1988).
- [26] S. Frixione, M. L. Mangano, P. Nason and G. Ridolfi, Phys. Lett. B **348**, 633 (1995).
- [27] J. J. Aubert *et al.* [European Muon Collaboration], Phys. Lett. B **123**, 275 (1983).
- [28] D. F. Geesaman, K. Saito and A. W. Thomas, Ann. Rev. Nucl. Part. Sci. **45**, 337 (1995).
- [29] G. Piller and W. Weise, Phys. Rept. **330**, 1 (2000).
- [30] N. Armesto, J. Phys. G **32**, R367 (2006).
- [31] V. J. Kolhinen, arXiv:hep-ph/0506287.
- [32] K. J. Eskola, V. J. Kolhinen and C. A. Salgado, Eur. Phys. J. C **9**, 61 (1999).
- [33] D. de Florian and R. Sassot, Phys. Rev. D **69**, 074028 (2004).
- [34] M. Hirai, S. Kumano and T. H. Nagai, Phys. Rev. C **70**, 044905 (2004); Nucl. Phys. Proc. Suppl. **139**, 21 (2005).
- [35] M. Hirai, S. Kumano and T. H. Nagai, Phys. Rev. C **76**, 065207 (2007).
- [36] K. J. Eskola, H. Paukkunen and C. A. Salgado, JHEP **0807**, 102 (2008).
- [37] K. J. Eskola, H. Paukkunen and C. A. Salgado, JHEP **0904**, 065 (2009).
- [38] I. Schienbein, J. Y. Yu, K. Kovarik, C. Keppel, J. G. Morfin, F. Olness and J. F. Owens, Phys. Rev. D **80**, 094004 (2009).
- [39] T. Stavreva, I. Schienbein, F. Arleo, K. Kovarik, F. Olness, J. Y. Yu and J. F. Owens, JHEP **1101**, 152 (2011).
- [40] K. Kovarik, I. Schienbein, F. I. Olness, J. Y. Yu, C. Keppel, J. G. Morfin, J. F. Owens and T. Stavreva, Phys. Rev. Lett. **106**, 122301 (2011).
- [41] D. de Florian, R. Sassot, P. Zurita and M. Stratmann, Phys. Rev. D **85**, 074028 (2012) [arXiv:1112.6324 [hep-ph]].
- [42] L. Frankfurt, V. Guzey and M. Strikman, Phys. Rev. D **71**, 054001 (2005).
- [43] L. Frankfurt, V. Guzey and M. Strikman, Phys. Rept. **512**, 255 (2012).
- [44] A. D. Martin, W. J. Stirling, R. S. Thorne and G. Watt, Eur. Phys. J. C **63**, 189 (2009).
- [45] D. W. Duke and J. F. Owens, Phys. Rev. D **26**, 1600 (1982).
- [46] M. Drees and K. Grassie, Z. Phys. C **28**, 451 (1985).
- [47] H. Abramowicz, K. Charchula and A. Levy, Phys. Lett. B **269**, 458 (1991).
- [48] K. Hagiwara, M. Tanaka, I. Watanabe and T. Izubuchi, Phys. Rev. D **51**, 3197 (1995).
- [49] M. Gluck, E. Reya and A. Vogt, Phys. Rev. D **45**, 3986 (1992).
- [50] M. Gluck, E. Reya and M. Stratmann, Phys. Rev. D **51**, 3220 (1995).
- [51] M. Gluck, E. Reya and A. Vogt, Phys. Rev. D **46**, 1973 (1992).
- [52] L. E. Gordon and J. K. Storrow, Nucl. Phys. B **489**, 405 (1997).
- [53] L. E. Gordon and J. K. Storrow, Z. Phys. C **56**, 307 (1992).
- [54] G. A. Schuler and T. Sjostrand, Phys. Lett. B **376**, 193 (1996).
- [55] G. A. Schuler and T. Sjostrand, Z. Phys. C **68**, 607 (1995).
- [56] P. Aurenche, J. P. Guillet and M. Fontannaz, Z. Phys. C **64**, 621 (1994).
- [57] P. Aurenche, P. Chiappetta, M. Fontannaz, J. P. Guillet and E. Pilon, Z. Phys. C **56**, 589 (1992).
- [58] F. Cornet, P. Jankowski, M. Krawczyk and A. Lorca, Phys. Rev. D **68**, 014010 (2003).
- [59] F. Cornet, P. Jankowski and M. Krawczyk, Acta Phys. Polon. B **35**, 2215 (2004).
- [60] F. Cornet, P. Jankowski and M. Krawczyk, Phys. Rev. D **70**, 093004 (2004).
- [61] P. Aurenche, M. Fontannaz and J. P. Guillet, Eur. Phys. J. C **44**, 395 (2005).
- [62] M. Strikman, R. Vogt and S. N. White, Phys. Rev. Lett. **96**, 082001 (2006).